Human Molecular Genetics, 2006, Vol. 15, No. 24 ***3578–3591***
doi:10.1093/hmg/ddl434

Mutant huntingtin inhibits clathrin-independent endocytosis and causes accumulation of cholesterol *in vitro* and *in vivo*

Eugenia Trushina[1,†], Raman Deep Singh[2,6,†], Roy B. Dyer[1], Sheng Cao[3,4], Vijay H. Shah[3,4], Robert G. Parton[7], Richard E. Pagano[2,5,6] and Cynthia T. McMurray[1,5,*]

[1]Department of Molecular Pharmacology and Experimental Therapeutics, [2]Department of Biochemistry and Molecular Biology, [3]Department of Internal Medicine and [4]Department of Physiology, Gastroenterology Research Unit and Tumor Biology Program, [5]Molecular Neuroscience Program and [6]Thoracic Diseases Research Unit Mayo Clinic, 200 First Street SW, Rochester, MN 55905, USA and [7]Institute for Molecular Bioscience and Centre for Microscopy and Microanalysis, University of Queensland, Queensland 4072, Australia

Received October 16, 2006; Revised and Accepted November 9, 2006

We show that the mutant Huntington's disease (HD) protein (mhtt) specifically inhibits endocytosis in primary striatal neurons. Unexpectedly, mhtt does not inhibit clathrin-dependent endocytosis as was anticipated based on known interacting partners. Instead, inhibition occurs through a non-clathrin, caveolar-related pathway. Expression of mhtt inhibited internalization of BODIPY-lactosylceramide (LacCer), which is internalized by a caveolar-related mechanism. In contrast, endocytosis of Alexa Fluor 594-transferrin (Tfn) and epidermal growth factor, internalized through clathrin pathway, was unaffected by mhtt expression. Caveolin-1 (cav1), the major structural protein of caveolae binds cholesterol and is responsible for its trafficking inside cells. Mhtt interacts with cav-1 and caused a striking accumulation of intracellular cholesterol. Cholesterol accumulated in cultured neurons expressing mhtt *in vitro* and in brains of mhtt-expressing animals *in vivo*, and was observed after induction of mhtt expression in PC-12 cell lines. The accumulation occurred only when mhtt and cav1 were simultaneously expressed in cells. Knockdown of cav1 in mhtt-expressing neurons blocked cholesterol accumulation and restored LacCer endocytosis. Thus, mhtt and cav1 functionally interact to cause both cellular defects. These data provide the first direct link between mhtt and caveolar-related endocytosis and also suggest a possible mechanism for HD neurotoxicity where cholesterol homeostasis is perturbed.

INTRODUCTION

Huntington's disease (HD) is a progressive neurodegenerative disorder with no cure (1). The normal function of huntingtin (htt) and the mechanism by which mutant huntingtin (mhtt) initiates striatal neurotoxicity are unclear. Studies on subcellular localization and identification of normal partners suggest that htt could function in vesicular trafficking and endocytosis (2). Yeast two-hybrid screens revealed that htt interacts with components of the trafficking machinery. Huntingtin-associated protein 1 (HAP1) was one of the first identified (3–5). Like htt, HAP1 is enriched in brain (3–5) and associates with microtubules and vesicles. HAP1 partially co-localizes with htt in cells and on sucrose gradient *in vitro* (6). Both htt and HAP1 interact with the trafficking motors, kinesin heavy chain and the dynactin $p150^{glued}$, an accessory protein for the microtubule motor protein dynein (3,4,7). In *Drosophila*, htt associates with Milton, a protein with homology to HAP1, which is also linked to kinesin-dependent axonal transport of mitochondria (8).

Functional evidence demonstrating that htt has a role in axonal trafficking has accumulated over the years. Early analysis revealed that htt together with HAP1 accumulated on either side of a crushed rat sciatic nerve, suggesting that htt was

*To whom correspondence should be addressed. Tel: +1 5072841597; Fax: +1 5072849111; Email: mcmurray.cynthia@mayo.edu
†The authors wish it to be known that, in their opinion, the first two authors should be regarded as joint First Authors.

actively transported, at least *in vitro*, from distant cellular sites in both retrograde and anterograde directions (6). Whether htt was a cargo or a transport accessory protein was not known at that time. Recently, compelling data obtained in mice (9), in *Drosophila* (10) and in isolated squid axoplasm (11) have provided direct functional evidence that htt itself is a trafficking protein, or, at least, strongly influences the process. In squid axoplasm, expression of a truncated polyglutamine fragment from the androgen receptor inhibits axonal trafficking 3-fold relative to wild-type. When the same peptide is expressed in dividing SYH-SY5Y cells, neurite outgrowth is prevented upon differentiation with retinoic acid and brain-derived neurotrophic factor, suggesting that trafficking defects are microtubule-dependent (11). The increased interaction of mhtt with HAP1 and dynactin $p150^{Glued}$ reduces the association of HAP1/dynactin $p150^{Glued}$ with taxol-stabilized microtubules assembled *in vitro*. Loss of axonal motility induced by mhtt appears to reduce the supply of important cargoes needed for synaptic transmission (12). In *Drosophila*, expression of mhtt also suppresses axonal transport of green fluorescence protein-tagged epidermal growth factor (EGF) receptor (10) or yellow fluorescence protein-tagged amyloid precursor protein (12), and promotes vesicle and organelle accumulation in axons. Axonal trafficking defects appear to be a direct consequence of mhtt. Expression of either truncated mhtt or expanded polyglutamine regions causes trafficking defects in isolated squid axoplasm where neither a nucleus nor protein synthesis is present (11).

The observations made in *Drosophila* essentially mimic those found in mammals (9,12). Expression of mhtt in mice destabilizes microtubule tracts in primary neurons and alters their morphology (13). As measured in real-time imaging experiments, expression of full-length mhtt in mouse models for HD results in defective axonal transport of vesicles and mitochondria very early in development (9). Importantly, vesicle transport and uptake of the retrograde dye, fluorogold, is suppressed in animals expressing mhtt with 72 polyglutamines. Two days after injection into live animals, the uptake of fluorogold in the mhtt-expressing mice is suppressed 3-fold relative to control animals (9). Thus, expression of the full-length endogenous form of mhtt in mice causes loss of trafficking both *in vivo* and *in vitro* and is not an artifact of cell dispersal.

The importance of trafficking, particularly in neurons, has raised the issue as to whether mhtt causes adverse defects at other steps of trafficking, which might contribute to toxicity. As with the axonal transport machinery, htt has been implicated in endocytosis based on its binding partners (2,14). Htt associates with clathrin, co-localizes with mature clathrin-coated vesicles and decorates clathrin-coated pits (15–17). Htt may form a complex with clathrin through Huntingtin-interacting protein 1 (HIP1) (18–21). HIP1 directly binds clathrin light chain, α-adaptin A and C and co-localizes with the clathrin coat adaptor, AP2 (19,22), which promotes actin binding and prevents depolymerization of actin filaments (23–25).

However, far less is known about the functional links between mhtt and endocytosis. Most of the existing data regarding endocytosis are based on effects of mhtt-interacting partners rather than mhtt itself. For example, loss of HIP1 in HIP1(−/−) mice causes a neurological deficit in endocytosis of alpha-amino-3-hydroxyl-5-isoxazolepropionate receptors (26). HAP1 regulates the decision of Gamma-aminobutyric acid type A receptors (GABA-AR) to recycle back to the cell surface or sort in the lysosome by inhibiting receptor degradation (27). However, in these experiments, a role for htt is implied rather than demonstrated. Moreover, no thorough examination of endocytosis has been conducted at the molecular level in primary striatal neurons, the most vulnerable in HD.

We have directly examined the effects of mhtt on endocytosis in primary striatal neurons from HD animals. We find that mhtt expression indeed inhibits endocytosis but, surprisingly, does so through a non-clathrin, caveolin-1-related pathway. Mhtt expression causes abnormal accumulation of cholesterol both *in vitro* and *in vivo*. Mhtt interacts with caveolin-1 (cav1), and this functional interaction appears to influence toxicity since reduction of cav1 expression in mhtt-expressing neurons blocks cholesterol accumulation and restores clathrin-independent endocytosis of BODIPY-lactosylceramide (LacCer).

RESULTS

Mhtt inhibits clathrin-independent endocytosis

To directly test whether expression of mhtt influences endocytosis, we monitored internalization of fluorescent endocytic markers in embryonic (E17) primary striatal neurons from control mice (28) and mice expressing full-length mhtt with 72 (HD72) (29) glutamines. In both lines, mhtt is expressed at endogenous levels driven by the endogenous promoter. The majority of cells (95%) were well-developed neurons (Fig. 1) as estimated by staining with neuron-specific βIII tubulin antibody (Fig. 1C) with less than 5% astroglial contamination [estimated by staining with glia-specific glial fibrillary acidic protein (GFAP) antibody] (data not shown). Neurons were previously characterized by the expression of synaptic proteins (9) and the presence of fully developed synaptic contacts (Fig. 1E and F). The majority of neurons represent GABAergic medium spiny projection neurons, 50% of which are enkephalin-positive (9,13,30,31). Using these cultures, we determined whether expression of mhtt had measurable effect on endocytosis.

Internalization by clathrin-dependent endocytosis was visualized using Alexa Fluor 594-labeled transferrin (Tfn) (Fig. 2), a well-characterized marker for this pathway (32). We also measured internalization of LacCer (Fig. 2), which is internalized by a caveolar-related mechanism in other cell types (33). To our surprise, we found that, in primary neurons, expression of mhtt had no effect on internalization of Tfn but, instead, inhibited entry of LacCer (Fig. 2A and B). In neurons and glial cells from HD72 mice, uptake of LacCer was inhibited 70% relative to control (Fig. 2B). Inhibition of endocytosis was not limited to LacCer. Internalization of fluorescent albumin, another marker for clathrin-independent, caveolar-related endocytosis, was also inhibited similar to that shown in some other cell types (33,34) (Fig. 2B). Under the same conditions, we observed no effect on internalization of fluorescently labeled epidermal growth factor (EGF), a marker for

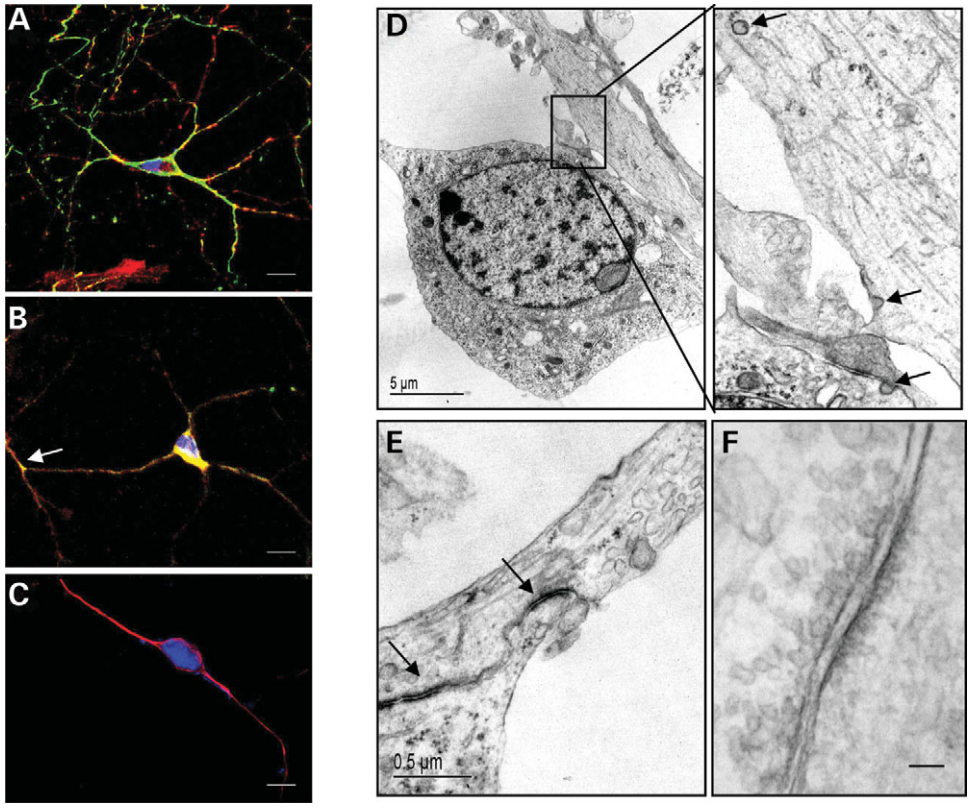

Figure 1. Integrity of the E17 primary striatal neurons. Confocal images of striatal neurons (7 DIC) co-stained with DAPI as a nuclear stain (blue), and (**A**) tubulin (green) and actin (red) antibodies, (**B**) kinesin (red) and dynactin (green) antibodies; white arrow indicates a synapse, (**C**) tubulin (red). Scale bar, 10 μm. (**D**) Electron micrograph of control neuron showing cell body and neurites; box is magnified on right; arrows in inset indicate clathrin-coated pits and vesicles. Formation of clathrin-coated vesicles occurred to the same extent in striatal neurons from both control and HD72 animals. Scale bar, 5 μm. (**E**) Electron micrograph of striatal neuron from control mice showing synaptic integrity. Synaptic contacts are dark regions indicated by the arrows. Scale bar, 0.5 μm. (**F**) Both control and HD72 neurons (7 DIC) develop synaptic contacts observed as darkly stained areas of the plasma membranes with formation of the synaptic vesicles. HD72 neuron is shown. Scale bar, 100 nm.

clathrin-dependent endocytosis (Fig. 2B). No differences were found in control and HD72 neurons in internalization of fluorescent dextran, the marker for fluid phase endocytosis (35) (Fig. 2B). These results indicated that expression of mhtt selectively inhibited internalization via a clathrin-independent pathway, whereas other pathways of uptake were apparently not affected.

To further characterize the mechanism of marker internalization in neurons, we tested the effects of pharmacological inhibitors (Fig. 2C and D). Chlorpromazine (CPZ), an inhibitor of clathrin-dependent endocytosis (34,36), blocked Tfn uptake by ~80% but had little effect on LacCer internalization (Fig. 2C and D). In contrast, pretreatment of cells with nystatin (specifically binds to plasma membrane cholesterol and flatten caveolae in other cell types) (37) inhibited LacCer uptake by ~80% with minimal effect on Tfn internalization. We also found that uptake of LacCer (but not Tfn) was blocked by Genistein (general tyrosine kinase inhibitor) or by PP2 (src kinase inhibitor) (Fig. 2D), as observed in other cell types when caveolar endocytosis is disturbed by specific inhibition of phosphorylation of its major structural protein, cav1 (33,38). Together, these results demonstrated that (i) in primary striatal neurons Tfn and EGF, and LacCer and Albumin, were internalized by distinctly different endocytic mechanisms, (ii) uptake of LacCer occurred through a clathrin-independent, caveolar-related pathway and (iii) expression of mhtt specifically inhibits endocytosis through a caveolar-related pathway.

Expression of mhtt causes accumulation of intracellular cholesterol *in vitro* and *in vivo*

Caveolae are characterized by their flask-shaped morphology and are defined by the presence of cav1 (39). However, the presence of caveolae in neurons has been controversial. To test whether striatal neurons have caveolar machinery, we determined whether cav1 was expressed in pure cultures of striatal neurons (glia $<5\%$), glial cultures and striatal brain tissue from control and mhtt-expressing mice (Fig. 3). Using specific antibodies, we found that cav1 was expressed in striatal neurons and glial cells from control or HD72 mice as measured by western blot analysis (Fig. 3A). We could also detect cav1 in cultures of striatal tissue (Fig. 3B). In all of these samples, cav1 migrated as a 22 kDa protein indistinguishable from cav1 found in control endothelial cells (Fig. 3A and B, En) and in hippocampal neurons (Fig. 3A, Hip) (40). Importantly, the level of cav1 expression in HD72 mice was not affected by expression of mhtt (Fig. 3A and B)

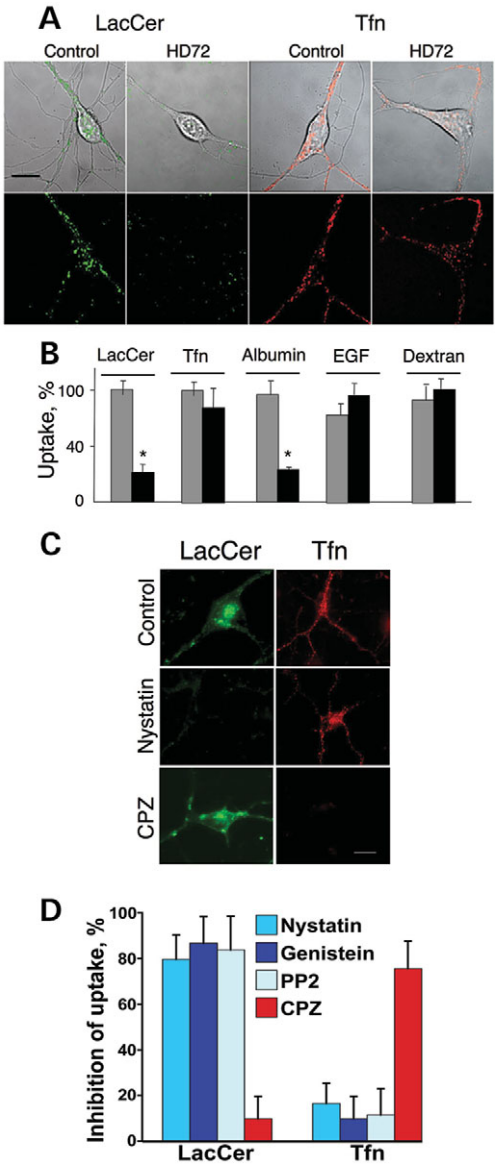

Figure 2. Clathrin-independent endocytosis is selectively inhibited in primary striatal neurons expressing mhtt. (**A**) Differential internalization of BODIPY-LacCer (green) and Alexa Fluor 594-Tfn (red) in living primary striatal neurons from control and HD72 mice. Experiments were performed on neurons 7 days after plating and neurons were visualized by confocal microscopy. Optical sections are 0.5 μm. Scale bar, 10 μm. (**B**) Internalization of additional fluorescent markers for clathrin and caveolar endocytic pathways in neurons from control (gray bars) and HD72 (black bars) mice. Data were obtained using conventional fluorescence and are expressed as percent of uptake relative to the control cells. Data represent quantification of at least 30 cells from three to 10 independent experiments. $^{*}P < 0.001$. (**C**) Characterization of LacCer and Tfn endocytic pathways in striatal neurons. Application of pharmacological inhibitors indicates that internalization of Tfn and LacCer in striatal neurons displays properties characteristic of clathrin-dependent and cav1-related pathways, respectively. Experiments were performed on control neurons 7 days after plating. Fluorescence images represent internalization of BODIPY-LacCer (LacCer) and Alexa Fluor 594-Tfn (Tfn) in live neurons from control mice with and without drug treatment. Nystatin (non-clathrin, caveolar-related pathway inhibitor) and CPZ (clathrin-dependent pathway inhibitor) are indicated. Scale bar, 10 μm. (**D**) Quantification of inhibition of fluorescent LacCer and Tfn internalization in control primary striatal neurons pretreated with pharmacological inhibitors, Nystatin and CPZ as in (C), Genistein (general tyrosine kinase inhibitor) and PP2 (src kinase inhibitor). Data were obtained by image analysis and are expressed relative to uptake seen in untreated control samples. Values are the mean ± SD of at least 30 cells in three independent experiments.

or by the age of the animals tested (Fig. 3B). Immunohistochemistry confirmed that cav1 was present along the plasma membrane of neurons. Antibody staining was specific since competing peptides blocked the fluorescence signal (data not shown), and no staining was observed in primary striatal neurons isolated from a cav1 knockout (CavKO) mouse (41) (Fig. 3C, CavKO). Thus, striatal neurons from control and HD72 mice possessed components required for caveolar-related endocytosis. Despite the abundance of cav1, however, we were unable to detect structures with the classic morphology of caveolae in either control or mhtt-expressing striatal neurons by electron microscopy. No caveolae were observed using electron microscopy in neurons at different times of maturation in culture [2, 6 and 8 days in culture (DIC)] or 2, 5 and 10 min after LacCer addition. Under all of these conditions, clathrin-coated vesicles were readily detected and to the same extent observed in neurons from both control and HD72 mice (Fig. 1D). Thus, mhtt did not appear to inhibit LacCer endocytosis by interfering with the formation of caveolae vesicles *per se*.

Cav1 directly binds cholesterol and is involved in its intracellular trafficking of caveolar vesicles (42,43). If mhtt caused inhibition of endocytosis through a cav1-related pathway, then intracellular trafficking of cholesterol might also be altered. To test this hypothesis, we stained striatal neurons with filipin, a polyene antibiotic that specifically binds free cholesterol, and measured its level by fluorescence microscopy (42). Indeed, we observed a striking and aberrant accumulation of cholesterol in neurons expressing mhtt (Fig. 4A). Within 12 days after plating, intracellular cholesterol in HD72 neurons accumulated up to 4-fold relative to control cells (Fig. 4B). This phenomenon was not accompanied by accumulation of cholesterol in the medium. Cholesterol accumulation in cultured neurons did not depend on the exogenous cholesterol. Intracellular accumulation was observed whether or not HD72 neurons were cultured in serum-containing or serum- and cholesterol-free medium (data not shown).

We found that cholesterol accumulation not only occurred in striatal neurons *in vitro* but also in the brains of HD72 mice *in vivo* and directly correlated with the age of the animals. We stained brain slices from 40-week-old animals with filipin (Fig. 4C, right) (44) and measured the level of cholesterol using fluorescence microscopy. Similar to the results in primary neurons, quantification of the filipin signal revealed an ~4-fold increase in cholesterol in HD72 mouse brains relative to controls (data not shown). As a second approach, we extracted the lipids from striata of control and HD72 mice (17, 24, 37 or 60 weeks of age) and quantified cholesterol levels by thin layer chromatography (45). In agreement with the filipin staining, a similar increase in intracellular cholesterol was measured in 60-week-old HD72 animals relative to 17-week-old animals (Fig. 4D). The age-related cholesterol accumulation occurred concomitantly with development of a clasping phenotype, an indicator of disease progression (Fig. 4C, left).

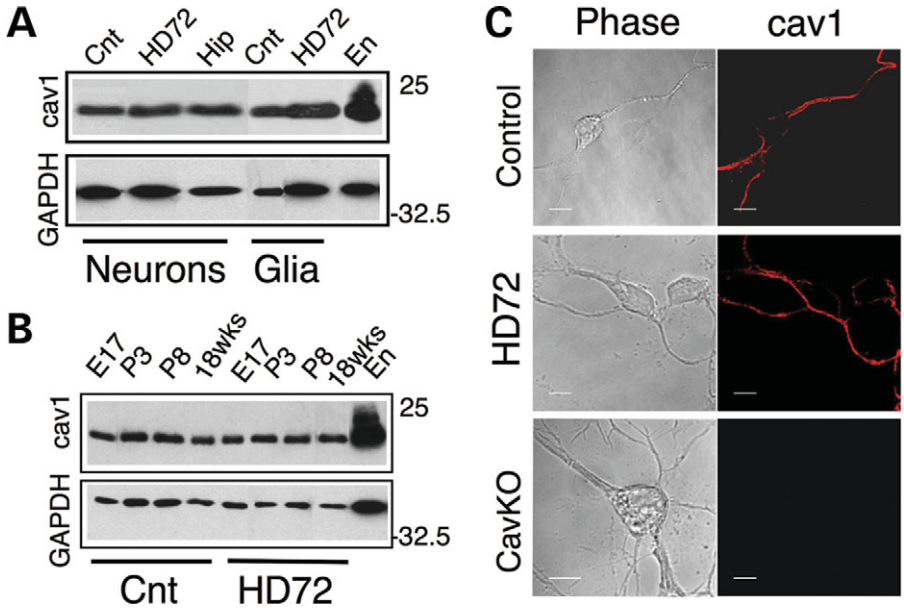

Figure 3. Cav1 is expressed in the striatum of control and HD72 mice. (**A**) Expression of cav1 in primary striatal neurons and glia from control (FVB/N) and HD72 mice detected with a polyclonal cav1 antibody. Cells were collected 7 days after plating. Neuronal cultures were obtained with 98% purity. Extracts from hippocampal neurons (Hip) and endothelial cells (En), both known to express cav1, were used as a control. Membranes were probed with GAPDH antibody for loading control. (**B**) Cav1 expression is maintained throughout animal development. Striatal tissue was extracted from age- and gender-matched control (FVB/N) and HD72 mice at embryonic day 17 (E17), postnatal days 3 (P3) and 8 (P8) and at 18 weeks of age (18 weeks). Tissue extracts were subjected to western analysis with cav1 polyclonal antibody. GAPDH staining was used as a loading control. En indicates endothelial cell lysate, a positive control for cav1. (**C**) Fluorescence and phase images of striatal (E17) neurons from FVB/N (control), HD72 and cav1 knockout mice (CavKO) at 7 days in culture labeled with a cav1 monoclonal antibody. The monoclonal antibody specifically recognizes cav1 on the plasma membrane. However, expression was also detected throughout the cell using a panel of three different cav1 polyclonal antibodies (Fig. 6). No cav1 was detected in CavKO neurons using any of the antibodies. Images were acquired using LSM 510 confocal microscope. Scale bar, 10 μm.

Accumulation of intracellular cholesterol depends on expression of mhtt

We next asked whether the effects observed in mhtt-expressing neurons and HD72 animals were direct consequences of mhtt expression. We developed PC-12 cell lines in which expression of endogenous levels of human full-length htt (26Q) or mhtt (82Q) could be induced upon addition of doxycycline (Dox), and low to undetectable levels of 26Q or 82Q were detected in the absence of Dox. To more closely mimic neurons, PC-12 cells were cultured in the presence of nerve growth factor (NGF) for 14 days (before Dox induction) until cells were fully differentiated and long processes were evident (Fig. 5A).

We found that the level of cholesterol accumulation correlated directly with mhtt expression. Both differentiated and non-differentiated cells expressing 82Q but not 26Q caused a striking increase in intracellular cholesterol indicating that cholesterol accumulation was a direct and specific consequence of mhtt expression (Fig. 5A–D). The rise in cholesterol occurred concomitantly with the rise in mhtt protein expression and was never observed when 26Q was expressed (Fig. 5A–D) or in the absence of induction. To follow reversibility of cholesterol accumulation in differentiated PC-12 cells, we induced mhtt expression for 2 days, removed Dox to stop protein expression and cells were assayed for protein levels (Fig. 5B and C) or fixed and stained with filipin at selected time points for up to 3 weeks (Fig. 5D). Full-length mhtt could be detected almost immediately after induction, but protein expression did approach maximum after 6–7 days (Fig. 5B and C). Cholesterol began to accumulate as mhtt expression approached its maximum, but the decline in mhtt expression was slow in the differentiated neuron-like cells, and preceded that of cholesterol by at least a week. Thus, mhtt expression appeared to induce a somewhat sustained cholesterol response (Fig. 5D).

We also found that induction of mhtt recapitulated the inhibition of LacCer uptake that we observed in primary neurons. PC-12 cells expressing 26Q and 82Q were tested at 13 days after Dox removal for the efficiency of internalization of fluorescent LacCer and Tfn. Indeed, confocal imaging revealed that Tfn was successfully internalized in all cells similar to primary neurons in both 26Q and 82Q (Fig. 5E and F). In contrast, internalization of LacCer was inhibited in cells expressing 82Q (Fig. 5E and F) and occurred concomitantly with the accumulation of cholesterol. Thus, induction of mhtt expression recapitulated both the inhibition of LacCer uptake and the cholesterol accumulation that we observed in primary neurons.

Mhtt interacts with cav1

We next considered potential mechanisms by which mhtt might alter caveolar-related endocytosis and cholesterol homeostasis. We discovered by three independent measures that mhtt interacted with cav1. First, confocal imaging revealed that mhtt co-localized with cav1 in striatal neurons (Fig. 6A). Using a panel of antibodies, we observed that cav1 was not only

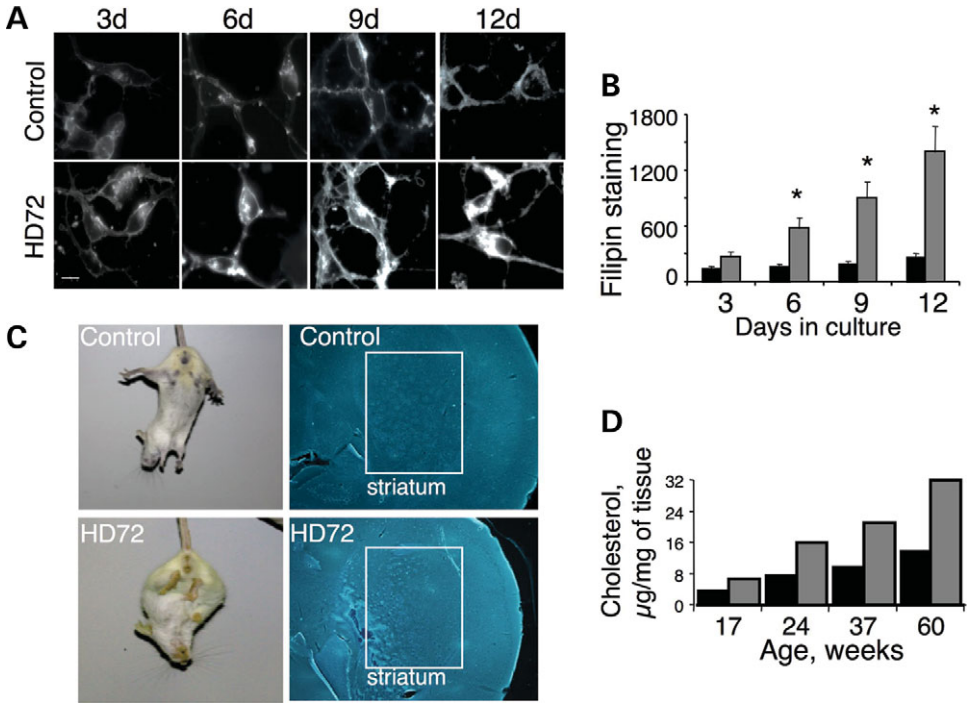

Figure 4. Cholesterol accumulates in striatal neurons and tissue *in vitro* and *in vivo*. (**A**) Fluorescence images of filipin staining in primary striatal neurons from control (FVB/N) and HD72 mice. Control and HD72 neurons were plated side by side, cultured in cholesterol-free medium, fixed at the days indicated and stained with filipin. Images were taken on an Olympus fluorescence microscope using 100× oil objective. Scale bar, 10 μm. (**B**) Quantification of filipin staining in striatal neurons from control (FVB/N) and HD72 mice at the indicated days *in vitro*. Values represent relative fluorescence units and are the mean ± SD of at least 30 cells in each of six independent experiments. $^{*}P < 0.001$. Black bars, control mice; gray bars, HD72. (**C**) Cholesterol accumulation in brain tissue of HD72 mice increases with age and correlates with progression of neurological abnormalities. (Right) Brain slices (30 μm) from control (FVB/N) and HD72 mice 40 weeks old stained with filipin. Box indicates the portion of striatum taken for quantitative analysis. HD72 mice display clasping phenotype (bottom left) absent in control mice (top left) that coincides with progressive accumulation of cholesterol in brain tissue [bottom right and (**D**)]. (D) Expression of mhtt causes accumulation of cholesterol in the striatum of HD72 mice *in vivo*. Striatal tissue was collected from control (FVB/N) and HD72 age-matched mice, cholesterol was extracted and measured using thin-layer chromatography (see Materials and Methods). Black bars, control mice; gray bars, HD72.

present along the plasma membrane (Fig. 3C, monoclonal antibody) but was also present throughout the cytoplasm (Fig. 6A, polyclonal cav1 antibody). When the same neuronal cultures were stained with antibodies specific for htt (2166 Ab), we found that cav1 co-localized with htt or mhtt both on the plasma membrane and in the cytoplasm (Fig. 6A). The level of co-localization was similar in HD72 and control neurons.

Second, to test whether co-localization was due to an interaction of cav1 with htt or mhtt, we performed parallel immunoprecipitation experiments. We found that antibodies to cav1 precipitated both htt and mhtt in mouse brain extracts (Fig. 6B, lanes 4 and 6). It is well documented that mhtt in cell extracts has slower migration on polyacrylamide gel relative to the wild-type htt (46,47), and the band can be less discreet due to multiple conformations of the polyglutamine tract. Therefore, mhtt and htt are readily resolved on SDS–PAGE gels. In control samples, the cav1 antibody immunoprecipitated only a single band corresponding to htt (Fig. 6B, lanes 2 and 4). In mhtt-containing samples, however, we observed a doublet indicating that cav1 interacted with both mhtt and htt (Fig. 6B, lane 6, mhtt indicated by a star). The reactions were specific for the primary antibody. Beads alone (Fig. 6B, lanes 1, 3 and 5) did not precipitate htt or mhtt nor were they immunoprecipitated in reactions using an unrelated hemagglutinin (HA) antibody (Fig. 6B, lane 7).

As a third measure, we tested whether mhtt and htt interacted with purified cav1. We expressed a full-length cav1–glutathione S-transferase (GST) fusion protein and immobilized it on glutathione-agarose. Beads containing either GST or GST–cav1 were incubated with extracts from striatal tissue from control and HD72 mice or from extracts prepared from pure cultures of striatal neurons. We evaluated the interacting proteins in a 'pull-down assay' (48). In agreement with immunoprecipitation studies, both htt and mhtt were pulled down with purified GST–cav1 (Fig. 6C). Consistent with the immunoprecipitation experiments, a single band was observed in tissue or neurons from control animals (Fig. 6C, lanes 3 and 4), whereas doublets corresponding to the htt and mhtt were detected in HD72 samples (Fig. 6C, lanes 5 and 6). These data demonstrated that purified cav1 interacted either directly with both htt and mhtt or indirectly with a complex containing these proteins.

Knockdown of cav1 expression in neurons from HD72 animals blocked cholesterol accumulation

To test whether an interaction of mhtt and cav1 was necessary for the cholesterol trafficking defect, we knocked down cav1 expression in neurons from HD72 animals by transfecting small interfering RNA (siRNA) for cav1 (siCav1). Transfection and internalization of the siRNA was highly efficient as

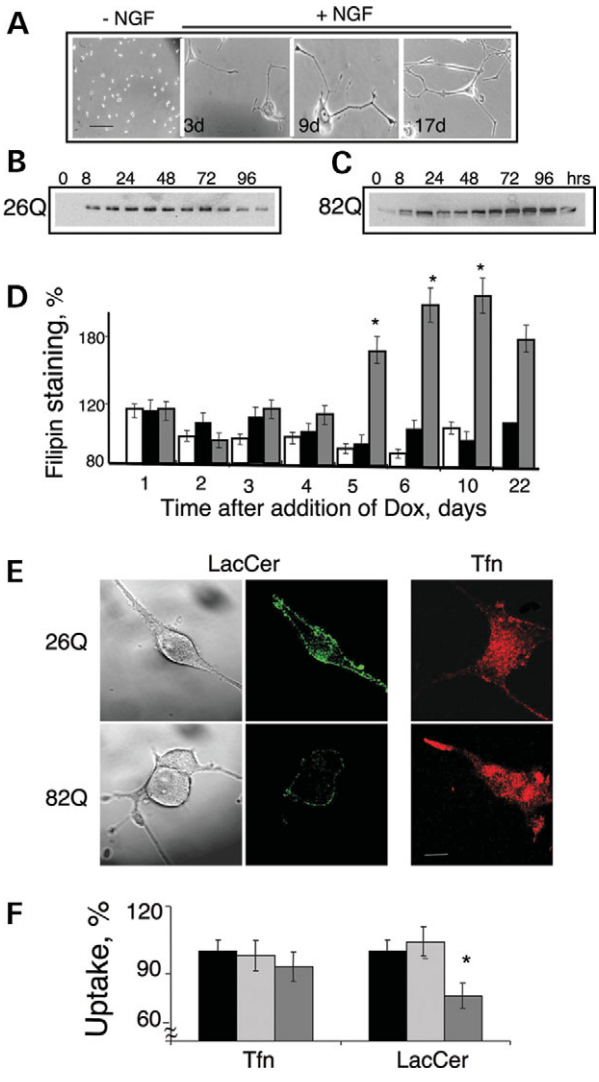

Figure 5. Inhibition of LacCer internalization and cholesterol accumulation in cells are a direct effect of mhtt expression. Analysis of mhtt expression and cholesterol accumulation in PC-12 Tet-On cells harboring a stable integration of full-length human htt (26Q) or mhtt (82Q). (**A**) Cells were differentiated to the neuronal phenotype. Both lines have little to no background expression without Dox and express similar levels of htt/mhtt upon Dox addition. Time course of 82Q (**B**) and 26Q (**C**) expression in differentiated PC-12 cells after induction with Dox for 48 h. Protein expression was measured by western blotting with the human specific htt antibody 2168 at the indicated times. (**D**) Cholesterol accumulation in differentiated parental PC-12 cells and cells expressing 26Q or 82Q in the presence (+Dox) and absence (−Dox) of Dox. Only cells expressing 82Q demonstrated increased cholesterol levels with time in culture. $^*P < 0.001$. White bar, parental PC-12 cells; black bar, 26Q; gray bar, 82Q. (**E**) Expression of 82Q inhibited the uptake of BODIPY-LacCer relative to 26Q but did not affect internalization of Alexa Fluor 594-Tfn. Images represent internal optical sections (0.5 μm) through a representative PC-12 cell at day 21 in culture. Internalization of BODIPY-LacCer was reduced in 82Q cells compared with 26Q or parental PC-12 cells (data not shown). Specifically, BODIPY-LacCer showed punctate staining throughout the cell in 26Q, but only surface labeling in 82Q cells. Tfn is detected as punctate staining throughout the cell in either cell line. Confocal images were obtained using LSM 510 microscope (Carl Zeiss, Germany); 100× oil DIC lens (1.4 n.a.), confocal slices were 0.5 μm. Laser excitation/emission was set to 543/560 nm (for Alexa Fluor 594-Tfn) and 488/550 nm (for BODIPY-LacCer). Scale bar, 10 μm. (**F**) Quantification of Alexa Fluor 594-Tfn and BODIPY-LacCer uptake in parental PC-12 cells and cells expressing 26Q and 82Q. $^*P < 0.001$. Black bar, parental PC-12 cells; striped bar, 26Q; gray bar, 82Q.

judged by the localization and intensity of the co-transfected siRNA-Glo marker (Dharmacon, Inc., Chicago, IL, USA) (Fig. 7A). Under these conditions, we found that cav1 expression was redcued by roughly 75% relative to untreated HD72 neurons after 10 DIC (Fig. 7D, Cav1 N20), whereas mhtt expression was not significantly altered (Fig. 7D, htt). Remarkably, we observed that neurons transfected by siCav1 failed to accumulate cholesterol relative to their untreated HD72 counterparts (Fig. 7B, C and E) or to wild-type FVB control neurons (data not shown). Moreover, rescue of the cholesterol trafficking defect by incubation with siCav1 was accompanied by restoration of LacCer endocytosis (Fig. 7F and H). Treatment with siCav1 did not alter Tfn endocytosis, which was normal in HD72 neurons (Fig. 7G). Thus, loss or reduction of cav1 reversed the defects in caveolar-related functions of endocytosis and intracellular cholesterol trafficking, despite the fact that the mhtt expression was maintained at equivalent levels.

DISCUSSION

Although, htt and mhtt interact with a number of clathrin coat proteins, we show here that mhtt does not inhibit clathrin-dependent endocytosis. Rather, our data indicate that inhibition occurs through a non-clathrin, caveolar-related pathway. This conclusion is supported by three key findings. In primary neurons, we find that mhtt inhibits internalization of LacCer, a marker for caveolar endocytosis, and impairs intracellular trafficking of cholesterol, a known caveolar-related function. The latter two effects occur in the brain tissues of whole animals as well as in dispersed cultured primary neurons from those animals. Inhibition of LacCer internalization and cholesterol accumulation appear to depend on the presence of both mhtt and cav1; cholesterol accumulation does not occur in cav1 expressing cells in the absence of mhtt, induction of mhtt in cav1 expressing cells casues both defects, and loss of cav1 in mhtt expressing cells restores normal function. In all of these cases, we observed little to no effect on internalization of classic clathrin-mediated cargo such as Tfn and EGF. Although the latter observation was unexpected, the results suggest plausible models.

First, an inhibitory role of mhtt on caveolar-related trafficking does not exclude a role of htt in clathrin-mediated endocytosis. In agreement with this notion, we find that loss of htt in striatal neurons inhibits Tfn uptake (Trushina *et al*., unpublished data). Second, the effects of mhtt on clathrin-mediated trafficking may occur, but not at the plasma membrane. HIP1 is a clathrin-coat protein also known to modulate endocytosis of GABA receptors and regulate inhibitory transmission (27). However, loss of HIP1 (and presumably loss of the htt/HIP1 interaction) does not influence Tfn entry into the cell (26). These data raise the possibility that the effects of mhtt on clathrin-mediated vesicular transport may be site-specific. Most htt interacting partners have been identified in yeast two-hybrid screens, which provide little information on when and where mhtt interactions might occur. However, even early work suggested that htt might operate at multiple intermediate steps in vesicle maturation (49,50). Overexpression of truncated HIP1 causes formation of large perinuclear vesicle-like structures containing HIP1, htt, clathrin and internalized transferrin (50). Thus, htt might

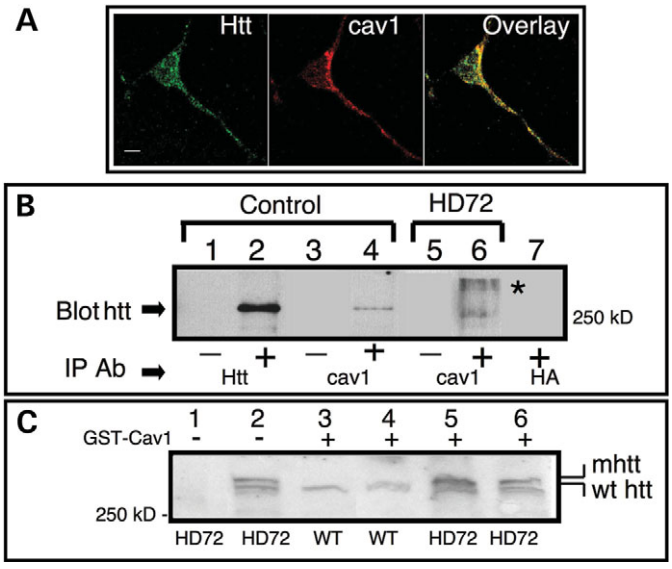

Figure 6. Cav1 interacts with both wild-type and mutant htt in striatal neurons and striatal tissue. (**A**) Htt and mhtt colocalize with cav1 in primary striatal neurons in cell body and neurites. Co-localization in control neurons is shown. Confocal images were taken using LSM 510 microscope with 63× (1.4 n.a.) DIC oil objective, focal plane was set to ~0.5 μm. Scale bar, 10 μm. Htt is green (monoclonal 2166), cav1 is red (polyclonal Ab). No differences were found in co-localization in HD72 neurons. (**B**) Cav1 antibody immunoprecipitated htt (lanes 4 and 6) and mhtt (lane 6, star) from brain extracts of control and HD72 mice. As a control, the 2170 htt antibody immunoprecipitated htt from control mouse brain (lane 2). Immunoprecipitates were detected by western blotting with htt 2166 Ab. (−) Protein-G beads without antibody (lanes 1, 3, 5), (+) protein-G beads crosslinked to htt Ab (lane 2) or cav1 Ab (lanes 4 and 6). HA is a control-unrelated antibody. (**C**) Both wild-type and mhtt interact with GST-fusion protein containing the full-length cav1 molecule. No interaction in the extracts from striatal tissue of HD72 mice was observed with GST alone (lane 1). Lane 2 represents positive control from striatal tissue of HD72 mice; double band corresponds to mhtt (upper band) and wild-type htt (lower band) as detected with htt 2166 antibody. GST–cav1 pull-down from both tissue lysates (lanes 3 and 5) and cell lysates (lanes 4 and 6) from control (FVB/N) and HD72 mice suggest that htt and mhtt interact with cav1. Equivalent amounts of GST and GST–cav1 were utilized as the substrate for binding.

regulate early to late endosome fusion events. Moreover, HIP1 organizes clathrin-coat proteins and stimulates their assembly through its conserved C-terminal domain, known as the I/LWEQ module (23–25). The I/LWEQ module of HIP1 promotes both its dimerization with HIP1R and its association with the plasma membrane via HIP1R binding to F-actin (51). Recently, it has been reported that HEAT domains directly bind membranes through electrostatic interactions with acidic phospholipids such as phosphatidylinositol 4,5-bisphosphate (52). As an interacting partner of HIP1R, htt might also act at the interface between actin filaments and the lipids of the plasma membrane. Thus, htt or mhtt interactions with clathrin and other trafficking machinery appear to be dynamic and multi-faceted, and the effects of mhtt at the initial events of endocytosis may be, at least, partially separable from downstream events.

Cholesterol is essential for promoting synapse formation and maintaining membrane integrity in CNS neurons (53,54). Moreover, defects in caveolae and/or perturbation of cholesterol homeostasis have been increasingly implicated in toxic mechanisms for Alzheimer's disease (AD), Parkinson's disease, Niemann–Pick Type C and other lipid storage diseases (55–60). Our discovery that mhtt inhibits caveolar-related endocytosis and causes accumulation of cholesterol potentially links HD and other neurodegenerative diseases. In rodent brain, depletion or accumulation of cholesterol can cause neurodegeneration with AD-like symptoms (55). In prion disease, glycosylphosphatidylinositol anchoring of prion protein (PrP) in the endoplasmic reticulum directs the PrP to the Golgi into cholesterol-rich caveolae-like domains. In caveolae, degradation of PrP slows and appears to be cholesterol sensitive (61). On the basis of these data, Prusiner and coworkers have raised the possibility that caveolae may be the sites of PrP misfolding facilitating its conversion to the aggregated, pathogenic form (61).

Our *in vitro* and *in vivo* data demonstrate that inhibition of caveolar-related endocytosis and consequent cholesterol accumulation arises directly from mhtt expression. In other reports, microarray data indicate that transcription of cholesterol biosynthetic enzymes is diminished in human postmortem HD brain (62) and that cholesterol is low in the brains of R6/2 mice (63). Thus, both sets of data agree that cholesterol homeostasis is perturbed by mhtt expression. Unlike HD72 animals, however, toxicity in R6/2 mice is acute and these animals die by 12 weeks. Thus, accumulation of cholesterol may occur early when symptoms are minimal, as in HD72 animals, but synthesis is impaired at later stages in the disease progression as animals or humans approach death. In any case, defects in caveolar-related trafficking and cholesterol accumulation are likely to be relevant to the pathophysiology of HD.

MATERIALS AND METHODS

Animals

All procedures involving animals were approved by the Institutional Animal Care and Use Committee. The following mouse models were used: control FVB/N (28) with seven glutamines in mouse endogenous htt homolog, homozygous transgenic with full-length human HD cDNA containing 72 (HD72) (29) CAG repeats (model was constructed using FVB/N mouse strain), cav1 null mice (CavKO) (41) and its parental strain C57BL/6J (Bl6).

Antibodies and immunocytochemistry

Primary antibodies were: mouse monoclonal cav1 (1:50, BD Transduction Laboratories, KY, USA), rabbit polyclonal cav1 H-97 (1:200) and N-20 (1:200, Santa Cruz Biotechnology, Inc., Santa Cruz, CA, USA), rabbit polyclonal cav1 (1:100, BD Transduction Laboratories), rabbit polyclonal α-synapsin (1:500, gift from Dr P. McPherson), rabbit anti-GABA (γ-aminobutyric acid) (1:12 000, Sigma, St Louis, MO, USA), mouse anti-βIII tubulin (Promega, Madison, WI, USA), mouse anti-GFAP Cy3 conjugated (1:400, Sigma). Secondary antibodies were: goat anti-mouse Cy 5 (1:1500, Amersham), goat anti-mouse TMR (1:400), goat anti-rabbit Cy5 (1:1500) and goat anti-rabbit TMR (1:50, Molecular Probes, Eugene, OR, USA). For blocking experiments, cav1 monoclonal or polyclonal antibodies were preincubated with specific blocking

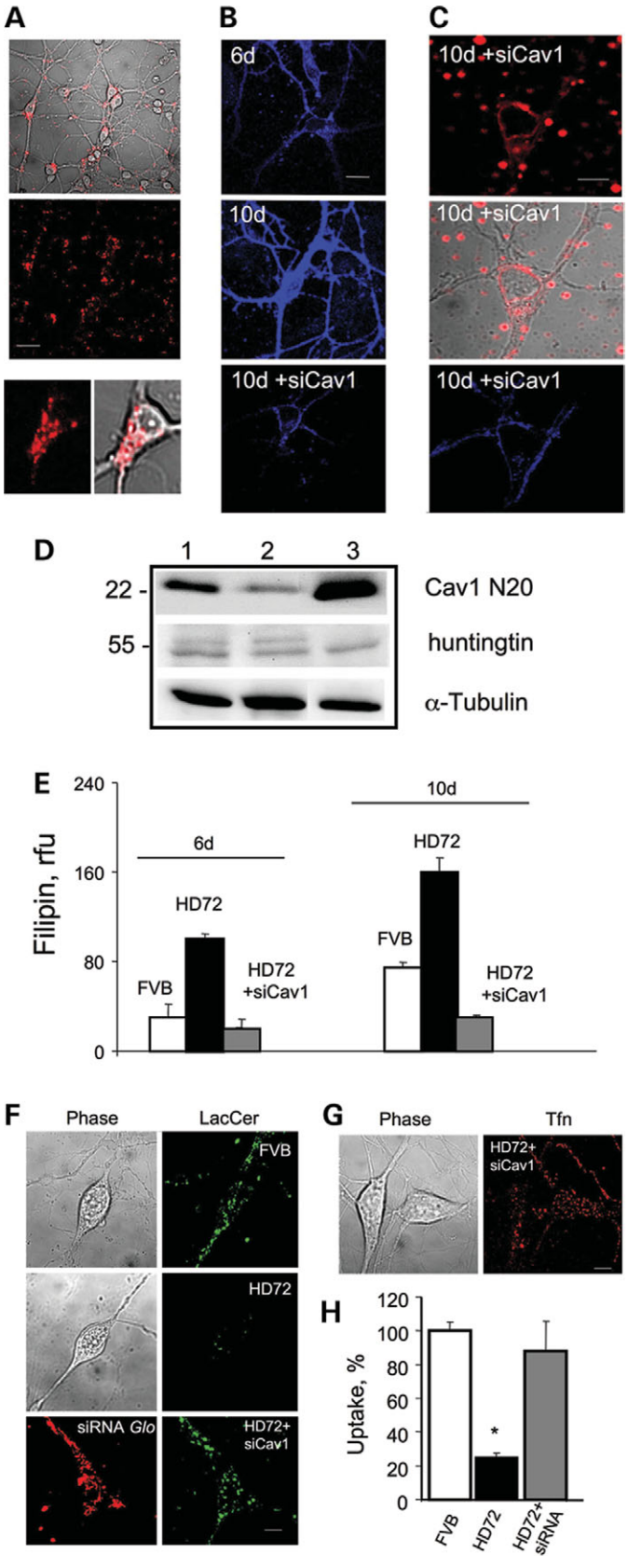

peptides overnight according to manufacture's protocol. Co-localization of htt and cav1 was examined using mouse anti-htt monoclonal antibody 2166 (1:300, Chemicon, CA, USA) and rabbit polyclonal cav1 H-97 (1:200). Immunostaining was performed as described previously (13,30).

Preparation of neuronal cell cultures

Preparation and culturing of primary striatal neurons were performed as described previously (13 in Supplementary Material). Briefly, mice were anesthetized with ether on gestational day 17 and fetuses were rapidly removed. Fetal brains were extracted and placed in sterile HEPES-buffered saline (HBS) (pH 7.3). The ventral part of the medial ganglionic eminence (the developmental precursor to the striatum) was dissected under a microscope. Tissue was placed in 1 mg/1 ml papain (Warthington, NJ, USA) in HBS for 20 min at 37°C. After two washes in HBS, the dissociated tissue was triturated in Dulbecco's modified Eagle's medium (DMEM) containing 10% Ham's F12 with glutamine (Gibco/BRL, Grand Island, NY, USA), 10% heat inactivated fetal calf serum (Hyclone Laboratories Logan, UT, USA) and 1× pen/strep antibiotic mixture. Cells were counted, diluted to 3×10^5 cells/ml, and 2 ml of this stock was placed in each well of a six-well dish containing glass cover slips coated with poly-L-ornithine (1 mg/2 ml sterile borate buffer, pH 8.4). Plated cells were maintained in an incubator with 5% CO_2 at 37°C. After 72 h in culture, medium containing serum was replaced with a serum-free neurobasal (NB)-based medium (without glutamine, Gibco/BRL, Grand Island) containing 1× pen/strep antibiotic mixture and 1× B27 supplement (Gibco/BRL, Grand Island) (64). Quantification of neurons and glia using specific antibody staining (GFAP for astrocytes and neuron-specific βIII-tubulin) demonstrates that neurons represent 95% of cells present on the cover slip. In cases where experiments required especially pure neuronal cultures, cells were

Figure 7. siRNA knockdown of cav1 blocks cholesterol accumulation and restores LacCer endocytosis in striatal neurons from HD72 animals. (**A**) High efficiency of siRNA transfection in primary neurons. (Top) Transmission image of primary neurons transfected with si*GLO*. Red indicates the cytoplasmic localization of fluorescently (Cy3) labeled si*GLO* RISC-free non-targeting siRNA. Nearly all neurons are transfected using Dharma*FECT* 3 transfection reagent; (middle) fluorescence image si*GLO*-positive neurons (from image at the top). (Bottom) Representative confocal images of neurons transfected with si*GLO*. Optical sectioning demonstrates that si*GLO* resides inside cells in the cytoplasm. Scale bar, 10 μm. (**B**) Filipin (blue) staining in neurons cultured for the indicated number of days (d). Culturing neurons for 10 days in the presence of siCav1 blocks cholesterol accumulation. Scale bar, 5 μm. (**C**) Magnified image of 10d + siCav1 neuron from B co-localizing siGLO and Filipin. Cells taking up siCav1 do not accumulate cholesterol. Fluorescence (top) and transmission (middle) images of transfected cells (marked by si*GLO*, red); transfected neuron have reduced cholesterol (bottom). Scale bar, 5 μm. (**D**) Western blot of proteins from untreated and siCav1-treated HD72 neurons probed with specific antibodies for cav1 (N-20), a-tubulin or huntingtin, as indicated. Cav1 is knocked down roughly 75% of untreated cells. (**E**) Quantification of data from (B). (**F**) Internalization of BODIPY-LacCer (green) in primary neurons 10 DIC. FVB controls (top), HD72 (middle) and HD72 neurons treated with siCav1. Red is siGLO. (**G**) Endocytosis of Tfn is unaffected by siCav1 treatment in HD72 neurons; (left) transmission image; (right) fluorescence image of Alexa Fluor 594-labeled Tfn. (**H**) Quantification of LacCer uptake data from (F). Analysis represents combined data from three independent experiments where at least 10 cells were imaged. $^*P < 0.001$.

treated with cytosine β-D-arabinofuranoside (Ara-C, Sigma) to a final concentration of 2 μM after 3 and 5 DIC to suppress proliferation of the glia cells. Such conditions allowed obtaining fully developed pure striatal neurons exhibiting synaptic activity as judged by staining with synapsin antibody (9) and EM examination of synaptic contacts. All experiments were performed in neurons 6–7 DIC unless specifically stated. The purity of the neuronal preparations was established using a panel of specific antibodies. Neurofilamnet and GFAP intensity was used to establish that ~90% of cultures were medium spiny GABAergic projection neurons (30) with ~50% being enkephalin positive (31). Expression of cav1 by western blot was detected using rabbit polyclonal N20 cav1 antibody (1:3000, Santa Cruz). Monoclonal mouse GAPDH antibody was used for loading control (1:6000; Chemicon).

Inhibitors and fluorescent markers of endocytosis

C_5-BODIPY-fatty acid labeled analog of LacCer was synthesized and purified as described previously (65). Alexa Fluor 594-labeled albumin, Tfn and EGF were from Molecular Probes. Striatal neurons plated on poly-L-ornithine-coated glass cover slips were washed with HEPES-buffered MEM (10 mM HMEM) at room temperature and then incubated with BODIPY-LacCer for 10 min at 37°C in the incubator with 5% CO_2 to induce endocytosis. After incubation, the medium was replaced with ice-cold HMEM without glucose, and the culture dishes were transferred to a 10°C bath. Fluorescent lipid present at the cell surface was removed by incubating the cells (six times, 10 min each) with 5% fatty acid free BSA in HMEM without glucose at 10°C. For other experiments, cells were incubated with 7.5 μg/ml Alexa Fluor 594-labeled albumin, Tfn and EGF for 10 min at 37°C. Excess of fluorescent markers at the cell surface was removed by acid stripping (33). Primary neurons were treated with various inhibitors to differentiate clathrin-dependent from clathrin-independent endocytosis as described (66). For inhibition of clathrin-dependent endocytosis, samples were pretreated with 8 μg/ml CPZ; for disruption of caveolar endocytosis, cells were pretreated with 25 μg/ml nystatin. Cells were also preincubated in HMEM containing PP2 (10 nM) or Genistein (50 μM) for 1 h at 37°C. Inhibitors were present in all subsequent steps of experiments. The specificity of each inhibitor treatment was evaluated by monitoring the internalization of fluorescent LacCer and Tfn as endocytic markers. Cell viability was >90% for each inhibitor treatment as judged by Trypan blue staining.

Fluorescence and confocal microscopy

Fluorescence microscopy using an Olympus IX70 fluorescence microscope and quantitative image analysis were performed using 100× oil DIC objective as described (33). Cells were imaged using confocal laser scanning microscope LSM 510 (Carl Zeiss) with 100× or 63× oil DIC objective (1.4 n.a.) with optical section set to ~0.5 μm as described (13).

Immunoprecipitation

Htt monoclonal antibody 2170 (Chemicon, Inc.), cav1 antibody (N20, Santa Cruz Biotechnology, Inc.) and HA tag antibody (Y-11, Santa Cruz Biotechnology, Inc.) were used. Antibodies were absorbed to Protein A/G Agarose Plus (Santa Cruz Biotechnology, Inc.) for 1 h at room temperature. Agarose beads were washed three times with 1 ml of 0.1 M sodium phosphate buffer, pH 7.0 and twice with 1 ml of 0.2 M triethanolamine, pH 8.2. Antibodies were crosslinked to the agarose by addition of freshly prepared 20 mM dimethylpimelimidate × 2HCl in 0.2 M triethanolamine, pH 8.2. After incubation for 30 min at room temperature, beads were collected and washed with 1 ml of 50 mM Tris, pH 7.5 for 15 min, then washed three times with PBS-T [PBS containing 0.1% polyoxyethylenesorbitan monolaurate (Tween-20)]. Conjugates were stored in PBS-T at 4°C. For IP, freshly isolated mouse forebrain was placed in 10 ml/gm of lysis buffer (10 mM Tris, pH 7.5, 150 mM NaCl, 1 mM EDTA, 1 mM EGTA, 1% Triton X-100, 0.5% NP-40, 0.2 mM sodium orthovanadate, 2 μg/ml aprotinin, 2 μg/ml leupeptin, 1 μg/ml pepstatin, 1 mM PMSF). Tissue was homogenized with 5–10 s pulses from a sonicator (Sonifier, Branson), incubated on ice for 20 min, then clarified at 12 000*g* for 20 min at 4°C. Supernatant was adjusted to 10% glycerol and stored at −20°C. Protein was quantified with the Advanced Protein Reagent (Cytoskeleton, Inc.). Two-hundred and forty micrograms of extract was brought to 1 ml with lysis buffer and 15 μl of 2166 or 10 μl of cav1 agarose conjugate was added. To control for non-specific absorption to the agarose, mock conjugated A/G Plus Agarose was added to the lysate. Reactions were incubated for 19–22 h with rocking at 4°C. Agarose was collected by microcentrifugation at 8160 g for 30 s. Supernatants were removed and agarose was washed three times with TNT buffer (10 mM Tris, pH 8.0; 140 mM NaCl; 0.1% Triton X-100), once with TN buffer (10 mM Tris, pH 8.0; 140 mM NaCl) and once with 50 mM Tris, pH 6.8. Agarose was resuspended in 40 μl of SDS sample buffer (58.3 mM Tris pH 6.8; 1.67% SDS; 5% glycerol; 2.5% 2-mercaptoethanol; 0.002% Bromophenol blue) and heated at 55°C for 10 min. The agarose along with the lysate was loaded onto SDS–PAGE gels for immunoblotting. Htt was detected with monoclonal antibody 2166 and cav1 was detected with polyclonal antibody N-20.

Interaction of wild-type or mutant htt with GST–cav1 fusion proteins

GST–cav1 fusion proteins were constructed and purified by affinity chromatography using glutathione-agarose as described (48). A total of 50 μg of GST or GST fusion proteins purified from *Escherichia coli* strain BL21 (DE3) LysS were bound to 20 μl of glutathione–Sepharose beads (Amersham Pharmacia Biotech) and incubated with 300 μl (~1 mg) of protein prepared from a lysis buffer containing 50 mM Tris (pH 7.5), 1% NP-40, 0.1% SDS, 0.1% sodium deoxycholate, 0.1 mM EGTA and 0.1 mM EDTA (with protease inhibitors), at 4°C for 2 h or overnight. Extracts from striatal tissue or pure striatal neurons (E17) from control (FVB/N) or transgenic HD72 mice have been used. To ensure complete separation of neurons from glia cells,

neurons after dissociation were preplated on the plastic 100 mm tissue culture dish for 3–5 h at 37°C and 5% CO_2. Such procedure allows glial cells to attach to the dish, whereas neurons will remain in suspension (neurons do not attach to the plastic unless a specific coating substrate such as poly-ornithine is used). Neurons were collected, spun down and frozen.

Unbound proteins were removed by five washes with a buffer containing 50 mM Tris (pH 7.7), 200 mM NaCl and 0.1 mM EDTA (with protease inhibitors). The specific bound proteins were released by resuspending beads in 30–50 μl of 2× SDS loading buffer and subjected to SDS–PAGE (4–20% polyacrylamide gel) and western blot analysis with mouse anti-htt 2166 (1:3000, Chemicon), rabbit anti-cav1 (1:1000, BD Transduction Laboratories) and anti-GST (1:2000, BD Pharmingen) specific antibodies. Horseradish peroxidase-conjugated anti-mouse (1:24 000) or anti-rabbit (1:2000, Chemicon) secondary antibodies were used to visualize bound proteins.

siRNA experiments

All reagents were from Dharmacon, Inc. Primary mouse striatal neurons were first evaluated for transfection efficiency using si*GLO* RISC-free non-targeting siRNA with fluorescent label (Cy3) and Dharma*FECT* 3 transfection reagent. Briefly, neurons from control and HD72 mice were plated on cover slips as described previously and cultured for 2 days in serum-containing medium. On day 3, the medium was substituted with NB-based serum-free, antibiotic-free medium. Twenty micromolar si*GLO* RNA in 1× siRNA buffer was used as a stock solution to prepare the final 100 nM siRNA solution in antibiotic-free, serum-free medium. To transfect three 35 mm dishes, we used the following protocol. In Tube 1, 17.5 μl of 20 μM siRNA was added to 612.5 μl of serum-free medium. In Tube 2, 14 μl of DharmaFECT 3 was added to 56 μl of serum-free medium. Contents of Tubes 1 and 2 were gently mixed and incubated at room temperature for 5 min. After that, Tubes 1 and 2 were mixed together, incubated 20 min at room temperature, 2.8 ml of fresh medium was added to bring the total volume to 3.5 ml. An aliquot of 1.0 ml of the transfection mixture was added to the neurons, and cells were observed under fluorescent microscope every other day up to 14 days. Cells were fed with fresh antibiotic- and serum-free medium every third day after transfection by adding 1 ml of medium to the dish. The identical protocol was used to introduce mouse cav1 ON-TARGETplus SMARTpool siRNA into neurons. Part of the experiments was performed with cav1 siRNA alone, part using si*GLO* siRNA as a co-transfection reagent with cav1 siRNA to identify transfected neurons in experiments using filipin staining. Additional neurons were transfected with cav1 siRNA to evaluate the suppression of cav1 expression by western blot. All experiments were performed in triplicates and repeated with two different platings.

Filipin staining in neurons and mouse brain sections

Striatal neurons from control and HD72 mice were plated on poly-ornithine-covered glass cover slips in six-well culture dishes in the serum containing medium and cultured for 3 days. Medium was switched to NB (cholesterol-free) medium, and cells were cultured for additional 12 days. Every third day after switch, 1 ml of medium in the cell culture dish was replaced with 1 ml of fresh NB medium. Cells were fixed with 4% paraformaldehyde (PFA) on days 3, 6, 9 and 12 after switch. Cover slips were washed three times with PBS, incubated 30 min with glycine (75 mg in 100 ml of PBS) and filipin solution (100 μg/ml, Polysciences, Inc., Warrington, PA, USA) was applied for 30 min at room temperature. Cells were washed in PBS and immediately observed under the fluorescence microscope using 100× magnification.

To evaluate the cholesterol levels in the brain, three control and three HD72 2-, 6- and 12-month-old female mice were deeply anesthetized with injection of 10 μl of 8 mg/ml Ketamine/1 mg/ml Xylazine per gram of the body weight. Brains were removed after mice were cardioperfused with freshly prepared 4% PFA. Sections were cut through caudate/putamen in frontal plane at 30 μm thick with an Oxford Vibratome. Sections were stained with filipin as described earlier. Filipin was detected using UV illumination (360–370 nm excitation, 420–460 nm emission) with an Olympus AX70 microscope under 10× magnification. To eliminate photobleaching while focussing and selecting cells or brain area for imaging, 90% neutrodensity filter with shattering system was used. For every mouse, cholesterol levels were acquired form six consecutive brain slices (12 hemispheres). Experiments in cells were repeated at least three times, 15–20 cells were examined for every time point. Statistical significance was determined using Student's *t*-test.

Cholesterol extraction from the brain tissue

Brain tissue from normal and HD72 mice was homogenized in 1 ml of PBS. About 100 μl of this suspension was used for protein estimation and remaining 900 μl was used for quantification of cholesterol. Cholesterol was extracted as described (45), and the lower organic phase containing lipids was collected and dried under N_2. The extracted lipids were then separated by TLC using $CHCl_3/C_2H_5OC_2H_5/CH_3COOH$, 65:15:1 (v/v/v) as the developing solvent for cholesterol. TLC plates were dried and then stained overnight with iodine. Cholesterol was quantified by densitometry and comparison with cholesterol standards run on the same TLC plate. Cholesterol content was normalized with protein and expressed as μg/mg of tissue.

Inducible PC-12 cell lines

PC-12 cells were stably transformed with 'reverse' Tet-regulated transcriptional activator (rtTA) construct that activates transcription of Tet-regulated genes in the presence of doxycycline (dox). Full-length human huntingtin cDNAs with 26 (control) and 82 (pathologic) glutamines were used to generate stable Tet-On cell lines. The huntingtin cDNAs were subcloned into the *Not*1 site of the pTRE-HA vector (BD Biosciences Clontech) after the vector was modified by replacing the region between the *Sfi*I and *Hin*dIII restriction sites with a linker oligo containing a BsiW1 restriction sequence. Proper orientation, frame and CAG length was con-

firmed by DNA sequencing. PC-12 cells stably transformed with reverse rtTA (BD Biosciences Clonetech) were co-transfected with the pTRE-Htt plasmids (4.7 μg) and pTK-Hyg (0.3 μg) (BD Biosciences Clonetech) for selection with hygromycin (100 μg/ml). Individual colonies were collected and analyzed for background expression and inducibility by doxycycline. Six wild-type and four mutant clonal lines were kept. Cells were maintained at 10% CO_2/37°C/100% humidity in DMEM supplemented with 10% horse serum, 5% fetal calf serum (Tet approved, Clontech), 100 μg/ml geneticin, 75 μg/ml hygromycin, 10 U/ml penicillin, 100 μg/ml streptomycin. For induction, PC-12 cells were plated on poly-ornithine-covered glass cover slips in DMEM with 5% fetal bovine serum and 10% horse serum. Cells were differentiated for 14 days by daily addition of NGF (100 ng/ml). Medium was changed to NB, and dox was added for 2 days at final concentration 100 ng/ml. After 2 days, dox was removed, and cells were allowed to stay in culture for 3 weeks. Cell at different time points after addition of dox were collected, and whole cell extracts were subjected to western blotting with htt 2168 monoclonal antibody that specifically recognized human htt (1:5000, Chemicon). Parental PC-12 cells and cells expressing 26Q and 82Q were fixed at different time points after dox addition and stained with filipin as described previously. Internalization of C_5-BODIPY-LacCer and Alexa Fluor 594-labeled Tfn was performed as described above for neurons with one exception. Since PC-12 cells at late time intervals very easily disattached from the cover slips upon washing or other manipulations, the removal of fluorescent lipid present at the cell surface was done by incubating the cells only three times 20 min each with 5% fatty acid free BSA in HMEM without glucose at 10°. This could explain residual fluorescence at the plasma membrane of the cells.

Statistical analysis

Data were analyzed using Student's *t*-test. $P < 0.01$ was considered statistically significant.

SUPPLEMENTARY MATERIAL

Supplementary Material is available at HMG Online.

ACKNOWLEDGEMENTS

We thank Dr C. Spiro for design, construction and characterization of the inducible PC-12 lines, Mr K. Johnson for help with mouse breeding, Mr T.A. Christensen and Dr J.L. Salisbury for help with electron microscopy and Mr T. Farnham for help with the manuscript. This work was supported by the Mayo Foundation, Hereditary Disease Foundation (CTM) and NIH grants NS40738 (CTM), R01 GM 066359 (CTM), GM-22942 (REP), GM-60934 (REP), R01-59615 and R01-59388 (VS), American Heart Association National Scientist Development Grant AHA04-35063N (SC).

Conflict of Interest Statement. None of the authors have any conflict of interest regarding any data described in the present paper.

REFERENCES

1. Bates, G., Harper, P., Jones, L. (eds) (2002) *Huntington's Disease*. Oxford University Press, New York.
2. Harjes, P. and Wanker, E.E. (2003) The hunt for huntingtin function: interaction partners tell many different stories. *Trends Biochem. Sci.*, **28**, 425–433.
3. Li, X.J. and Li, S.H. (2005) HAP1 and intracellular trafficking. *Trends Pharmacol. Sci.*, **26**, 1–3.
4. Li, S.H., Gutekunst, C.A., Hersch, S.M. and Li, X.J. (1998) Interaction of huntingtin-associated protein with dynactin P150Glued. *J. Neurosci.*, **18**, 1261–1269.
5. Li, S.H., Hosseini, S.H., Gutekunst, C.A., Hersch, S.M., Ferrante, R.J. and Li, X.J. (1998) A human HAP1 homologue. Cloning, expression, and interaction with huntingtin. *J. Biol. Chem.*, **273**, 19220–19227.
6. Block-Galarza, J., Chase, K.O., Sapp, E., Vaughn, K.T., Vallee, R.B., DiFiglia, M. and Aronin, N. (1997) Fast transport and retrograde movement of huntingtin and HAP 1 in axons. *Neuroreport*, **8**, 2247–2251.
7. Engelender, S., Sharp, A.H., Colomer, V., Tokito, M.K., Lanahan, A., Worley, P., Holzbaur, E.L. and Ross, C.A. (1997) Huntingtin-associated protein 1 (HAP1) interacts with the p150Glued subunit of dynactin. *Hum. Mol. Genet.*, **6**, 2205–2212.
8. Stowers, R.S., Megeath, L.J., Gorska-Andrzejak, J., Meinertzhagen, I.A. and Schwarz, T.L. (2002) Axonal transport of mitochondria to synapses depends on milton, a novel *Drosophila* protein. *Neuron*, **36**, 1063–1077.
9. Trushina, E., Dyer, R.B., Badger, J.D., II, Ure, D., Eide, L., Tran, D.D., Vrieze, B.T., Legendre-Guillemin, V., McPherson, P.S., Mandavilli, B.S. *et al*. (2004) Mutant huntingtin impairs axonal trafficking in mammalian neurons *in vivo* and *in vitro*. *Mol. Cell. Biol.*, **24**, 8195–8209.
10. Gunawardena, S., Her, L.S., Brusch, R.G., Laymon, R.A., Niesman, I.R., Gordesky-Gold, B., Sintasath, L., Bonini, N.M. and Goldstein, L.S. (2003) Disruption of axonal transport by loss of huntingtin or expression of pathogenic polyQ proteins in *Drosophila*. *Neuron*, **40**, 25–40.
11. Szebenyi, G., Morfini, G.A., Babcock, A., Gould, M., Selkoe, K., Stenoien, D.L., Young, M., Faber, P.W., MacDonald, M.E., McPhaul, M.J. *et al*. (2003) Neuropathogenic forms of huntingtin and androgen receptor inhibit fast axonal transport. *Neuron*, **40**, 41–52.
12. Gauthier, L.R., Charrin, B.C., Borrell-Pages, M., Dompierre, J.P., Rangone, H., Cordelieres, F.P., De Mey, J., MacDonald, M.E., Lessmann, V., Humbert, S. *et al*. (2004) Huntingtin controls neurotrophic support and survival of neurons by enhancing BDNF vesicular transport along microtubules. *Cell*, **118**, 127–138.
13. Trushina, E., Heldebrant, M.P., Perez-Terzic, C.M., Bortolon, R., Kovtun, I.V., Badger, J.D., II, Terzic, A., Estevez, A., Windebank, A.J., Dyer, R.B. *et al*. (2003) Microtubule destabilization and nuclear entry are sequential steps leading to toxicity in Huntington's disease. *Proc. Natl Acad. Sci. USA*, **100**, 12171–12176.
14. Paschen, W. and Mengesdorf, T. (2005) Endoplasmic reticulum stress response and neurodegeneration. *Cell. Calcium*, **38**, 409–415.
15. Mattson, M.P. (2002) Accomplices to neuronal death. *Nature*, **415**, 377–379.
16. Velier, J., Kim, M., Schwarz, C., Kim, T.W., Sapp, E., Chase, K., Aronin, N. and DiFiglia, M. (1998) Wild-type and mutant huntingtins function in vesicle trafficking in the secretory and endocytic pathways. *Exp. Neurol.*, **152**, 34–40.
17. Kim, M., Velier, J., Chase, K., Laforet, G., Kalchman, M.A., Hayden, M.R., Won, L., Heller, A., Aronin, N. and Difiglia, M. (1999) Forskolin and dopamine D1 receptor activation increase huntingtin's association with endosomes in immortalized neuronal cells of striatal origin. *Neuroscience*, **89**, 1159–1167.
18. Vecchi, M. and Di Fiore, P.P. (2005) It's HIP to be a hub: new trends for old-fashioned proteins. *J. Cell Biol.*, **170**, 169–171.
19. Engqvist-Goldstein, A.E., Kessels, M.M., Chopra, V.S., Hayden, M.R. and Drubin, D.G. (1999) An actin-binding protein of the Sla2/Huntingtin interacting protein 1 family is a novel component of clathrin-coated pits and vesicles. *J. Cell Biol.*, **147**, 1503–1518.
20. Wanker, E.E., Rovira, C., Scherzinger, E., Hasenbank, R., Walter, S., Tait, D., Colicelli, J. and Lehrach, H. (1997) HIP-I: a huntingtin interacting protein isolated by the yeast two-hybrid system. *Hum. Mol. Genet.*, **6**, 487–495.
21. Kalchman, M.A., Koide, H.B., McCutcheon, K., Graham, R.K., Nichol, K., Nishiyama, K., Kazemi-Esfarjani, P., Lynn, F.C., Wellington, C., Metzler, M. *et al*. (1997) HIP1, a human homologue of S. cerevisiae

Sla2p, interacts with membrane-associated huntingtin in the brain. *Nat. Genet.*, **16**, 44–53.
22. Waelter, S., Scherzinger, E., Hasenbank, R., Nordhoff, E., Lurz, R., Goehler, H., Gauss, C., Sathasivam, K., Bates, G.P., Lehrach, H. *et al*. (2001) The huntingtin interacting protein HIP1 is a clathrin and alpha-adaptin-binding protein involved in receptor-mediated endocytosis. *Hum. Mol. Genet.*, **10**, 1807–1817.
23. Legendre-Guillemin, V., Metzler, M., Lemaire, J.F., Philie, J., Gan, L., Hayden, M.R. and McPherson, P.S. (2005) Huntingtin interacting protein 1 (HIP1) regulates clathrin assembly through direct binding to the regulatory region of the clathrin light chain. *J. Biol. Chem.*, **280**, 6101–6108.
24. Chen, C.Y. and Brodsky, F.M. (2005) Huntingtin-interacting protein 1 (Hip1) and Hip1-related protein (Hip1R) bind the conserved sequence of clathrin light chains and thereby influence clathrin assembly *in vitro* and actin distribution *in vivo*. *J. Biol. Chem.*, **280**, 6109–6117.
25. Wesp, A., Hicke, L., Palecek, J., Lombardi, R., Aust, T., Munn, A.L. and Riezman, H. (1997) End4p/Sla2p interacts with actin-associated proteins for endocytosis in Saccharomyces cerevisiae. *Mol. Biol. Cell*, **8**, 2291–2306.
26. Metzler, M., Li, B., Gan, L., Georgiou, J., Gutekunst, C.A., Wang, Y., Torre, E., Devon, R.S., Oh, R., Legendre-Guillemin, V. *et al*. (2003) Disruption of the endocytic protein HIP1 results in neurological deficits and decreased AMPA receptor trafficking. *EMBO J.*, **22**, 3254–3266.
27. Kittler, J.T., Thomas, P., Tretter, V., Bogdanov, Y.D., Haucke, V., Smart, T.G. and Moss, S.J. (2004) Huntingtin-associated protein 1 regulates inhibitory synaptic transmission by modulating gamma-aminobutyric acid type A receptor membrane trafficking. *Proc. Natl Acad. Sci. USA*, **101**, 12736–12741.
28. Barnes, G.T., Duyao, M.P., Ambrose, C.M., McNeil, S., Persichetti, F., Srinidhi, J., Gusella, J.F. and MacDonald, M.E. (1994) Mouse Huntington's disease gene homolog (Hdh). *Somat. Cell Mol. Genet.*, **20**, 87–97.
29. Hodgson, J.G., Agopyan, N., Gutekunst, C.A., Leavitt, B.R., LePiane, F., Singaraja, R., Smith, D.J., Bissada, N., McCutcheon, K., Nasir, J. *et al*. (1999) A YAC mouse model for Huntington's disease with full-length mutant huntingtin, cytoplasmic toxicity, and selective striatal neurodegeneration. *Neuron*, **23**, 181–192.
30. Ventimiglia, R. and Lindsay, R.M. (1998) Characterizing and studying neuron cultures. In Banker, G. and Goslin, K. (eds), *Culturing Nerve Cells*, 2nd edn, Chapter 5, MIT Press, Cambridge, MA, 371–393.
31. Saudou, F., Finkbeiner, S., Devys, D. and Greenberg, M.E. (1998) Huntingtin acts in the nucleus to induce apoptosis but death does not correlate with the formation of intranuclear inclusions. *Cell*, **95**, 55–66.
32. Mukherjee, S., Ghosh, R.N. and Maxfield, F.R. (1997) Endocytosis. *Physiol. Rev.*, **77**, 759–803.
33. Singh, R.D., Puri, V., Valiyaveettil, J.T., Marks, D.L., Bittman, R. and Pagano, R.E. (2003) Selective caveolin-1-dependent endocytosis of glycosphingolipids. *Mol. Biol. Cell*, **14**, 3254–3265.
34. Schubert, W., Frank, P.G., Razani, B., Park, D.S., Chow, C.W. and Lisanti, M.P. (2001) Caveolae-deficient endothelial cells show defects in the uptake and transport of albumin *in vivo*. *J. Biol. Chem.*, **276**, 48619–48622.
35. Sabharanjak, S., Sharma, P., Parton, R.G. and Mayor, S. (2002) GPI-anchored proteins are delivered to recycling endosomes via a distinct cdc42-regulated, clathrin-independent pinocytic pathway. *Dev. Cell*, **2**, 411–423.
36. Gustavsson, J., Parpal, S., Karlsson, M., Ramsing, C., Thorn, H., Borg, M., Lindroth, M., Peterson, K.H., Magnusson, K.E. and Stralfors, P. (1999) Localization of the insulin receptor in caveolae of adipocyte plasma membrane. *FASEB J.*, **13**, 1961–1971.
37. Rothberg, K.G., Heuser, J.E., Donzell, W.C., Ying, Y.S., Glenney, J.R. and Anderson, R.G. (1992) Caveolin, a protein component of caveolae membrane coats. *Cell*, **68**, 673–682.
38. Sharma, D.K., Brown, J.C., Choudhury, A., Peterson, T.E., Holicky, E., Marks, D.L., Simari, R., Parton, R.G. and Pagano, R.E. (2004) Selective stimulation of caveolar endocytosis by glycosphingolipids and cholesterol. *Mol. Biol. Cell*, **15**, 3114–3122.
39. Schnitzer, J.E., Oh, P., Pinney, E. and Allard, J. (1994) Filipin-sensitive caveolae-mediated transport in endothelium: reduced transcytosis, scavenger endocytosis, and capillary permeability of select macromolecules. *J. Cell Biol.*, **127**, 1217–1232.
40. Bu, J., Bruckner, S.R., Sengoku, T., Geddes, J.W. and Estus, S. (2003) Glutamate regulates caveolin expression in rat hippocampal neurons. *J. Neurosci. Res.*, **72**, 185–190.
41. Razani, B., Engelman, J.A., Wang, X.B., Schubert, W., Zhang, X.L., Marks, C.B., Macaluso, F., Russell, R.G., Li, M., Pestell, R.G. *et al*. (2001) Caveolin-1 null mice are viable but show evidence of hyperproliferative and vascular abnormalities. *J. Biol. Chem.*, **276**, 38121–38138.
42. Simionescu, N., Lupu, F. and Simionescu, M. (1983) Rings of membrane sterols surround the openings of vesicles and fenestrae, in capillary endothelium. *J. Cell Biol.*, **97**, 1592–1600.
43. Fielding, C.J. and Fielding, P.E. (2001) Caveolae and intracellular trafficking of cholesterol. *Adv. Drug Deliv. Rev.*, **49**, 251–264.
44. Cuevas, P., Gutierrez Diaz, J.A., Dujovny, M., Diaz, F.G. and Ausman, J.I. (1988) Freeze-fracture cytochemistry of cholesterol content in neuronal plasma membrane following cerebral ischaemia. *Neurol. Res.*, **10**, 2–6.
45. Martin, O.C., Comly, M.E., Blanchette-Mackie, E.J., Pentchev, P.G. and Pagano, R.E. (1993) Cholesterol deprivation affects the fluorescence properties of a ceramide analog at the Golgi apparatus of living cells. *Proc. Natl Acad. Sci. USA*, **90**, 2661–2265.
46. Mangiarini, L., Sathasivam, K., Seller, M., Cozens, B., Harper, A., Hetherington, C., Lawton, M., Trottier, Y., Lehrach, H., Davies, S.W. *et al*. (1996) Exon 1 of the HD gene with an expanded CAG repeat is sufficient to cause a progressive neurological phenotype in transgenic mice. *Cell*, **87**, 493–506.
47. Dyer, R.B. and McMurray, C.T. (2001) Mutant protein in Huntington disease is resistant to proteolysis in affected brain. *Nat. Genet.*, **29**, 270–278.
48. Cao, S., Yao, J. and Shah, V. (2003) The proline-rich domain of dynamin-2 is responsible for dynamin-dependent *in vitro* potentiation of endothelial nitric-oxide synthase activity via selective effects on reductase domain function. *J. Biol. Chem.*, **278**, 5894–5901.
49. Sharp, A.H., Loev, S.J., Schilling, G., Li, S.H., Li, X.J., Bao, J., Wagster, M.V., Kotzuk, J.A., Steiner, J.P., Lo, A. *et al*. (1995) Widespread expression of Huntington's disease gene (IT15) protein product. *Neuron*, **14**, 1065–1074.
50. DiFiglia, M., Sapp, E., Chase, K., Schwarz, C., Meloni, A., Young, C., Martin, E., Vonsattel, J.P., Carraway, R., Reeves, S.A. *et al*. (1995) Huntingtin is a cytoplasmic protein associated with vesicles in human and rat brain neurons. *Neuron*, **14**, 1075–1081.
51. Senetar, M.A., Foster, S.J. and McCann, R.O. (2004) Intrasteric inhibition mediates the interaction of the I/LWEQ module proteins Talin1, Talin2, Hip1 and Hip12 with actin. *Biochemistry*, **43**, 15418–15428.
52. Kegel, K.B., Sapp, E., Yoder, J., Cuiffo, B., Sobin, L., Kim, Y.J., Qin, Z.H., Hayden, M.R., Aronin, N., Scott, D.L. *et al*. (2005) Huntingtin associates with acidic phospholipids at the plasma membrane. *J. Biol. Chem.*, **280**, 36464–36473.
53. Mauch, D.H., Nagler, K., Schumacher, S., Goritz, C., Muller, E.C., Otto, A. and Pfrieger, F.W. (2001) CNS synaptogenesis promoted by glia-derived cholesterol. *Science*, **294**, 1354–1357.
54. Hering, H., Lin, C.C. and Sheng, M. (2003) Lipid rafts in the maintenance of synapses, dendritic spines, and surface AMPA receptor stability. *J. Neurosci.*, **23**, 3262–3271.
55. Koudinov, A.R. and Koudinova, N.V. (2005) Cholesterol homeostasis failure as a unifying cause of synaptic degeneration. *J. Neurol. Sci.*, **229–230**, 233–240.
56. Koudinov, A.R. and Koudinova, N.V. (2001) Essential role for cholesterol in synaptic plasticity and neuronal degeneration. *FASEB J.*, **15**, 1858–1860.
57. Distl, R., Treiber-Held, S., Albert, F., Meske, V., Harzer, K. and Ohm, T.G. (2003) Cholesterol storage and tau pathology in Niemann–Pick type C disease in the brain. *J. Pathol.*, **200**, 104–111.
58. Puri, V., Watanabe, R., Dominguez, M., Sun, X., Wheatley, C.L., Marks, D.L. and Pagano, R.E. (1999) Cholesterol modulates membrane traffic along the endocytic pathway in sphingolipid-storage diseases. *Nat. Cell Biol.*, **1**, 386–388.
59. Bouillot, C., Prochiantz, A., Rougon, G. and Allinquant, B. (1996) Axonal amyloid precursor protein expressed by neurons *in vitro* is present in a membrane fraction with caveolae-like properties. *J. Biol. Chem.*, **271**, 7640–7644.
60. Hashimoto, M., Takenouchi, T., Rockenstein, E. and Masliah, E. (2003) Alpha-synuclein up-regulates expression of caveolin-1 and down-regulates extracellular signal-regulated kinase activity in B103 neuroblastoma cells: role in the pathogenesis of Parkinson's disease. *J. Neurochem.*, **85**, 1468–1479.
61. Peters, P.J., Mironov, A., Jr, Peretz, D., van Donselaar, E., Leclerc, E., Erpel, S., DeArmond, S.J., Burton, D.R., Williamson, R.A., Vey, M. *et al*.

(2003) Trafficking of prion proteins through a caveolae-mediated endosomal pathway. *J. Cell Biol.*, **162**, 703–717.
62. Sipione, S., Rigamonti, D., Valenza, M., Zuccato, C., Conti, L., Pritchard, J., Kooperberg, C., Olson, J.M. and Cattaneo, E. (2002) Early transcriptional profiles in huntingtin-inducible striatal cells by microarray analyses. *Hum. Mol. Genet.*, **11**, 1953–1965.
63. Valenza, M., Rigamonti, D., Goffredo, D., Zuccato, C., Fenu, S., Jamot, L., Strand, A., Tarditi, A., Woodman, B., Racchi, M. *et al*. (2005) Dysfunction of the cholesterol biosynthetic pathway in Huntington's disease. *J. Neurosci.*, **25**, 9932–9939.
64. Brewer, G.J., Torricelli, J.R., Evege, E.K. and Price, P.J. (1993) Optimized survival of hippocampal neurons in B27-supplemented Neurobasal, a new serum-free medium combination. *J. Neurosci. Res.*, **35**, 567–576.
65. Martin, O.C. and Pagano, R.E. (1994) Internalization and sorting of a fluorescent analogue of glucosylceramide to the Golgi apparatus of human skin fibroblasts: utilization of endocytic and nonendocytic transport mechanisms. *J. Cell Biol.*, **125**, 769–781.
66. Puri, V., Watanabe, R., Singh, R.D., Dominguez, M., Brown, J.C., Wheatley, C.L., Marks, D.L. and Pagano, R.E. (2001) Clathrin-dependent and -independent internalization of plasma membrane sphingolipids initiates two Golgi targeting pathways. *J. Cell Biol.*, **154**, 535–547.